Yali Zhang,[1] Charles M. Welzig,[2,3] Kristen L. Picard,[1] Chuang Du,[4] Bo Wang,[1] Jen Q. Pan,[5] John M. Kyriakis,[1] Mark J. Aronovitz,[1] William C. Claycomb,[6] Robert M. Blanton,[1,3] Ho-Jin Park,[1] and Jonas B. Galper[1,3]

Glycogen Synthase Kinase-3β Inhibition Ameliorates Cardiac Parasympathetic Dysfunction in Type 1 Diabetic Akita Mice

Diabetes 2014;63:2097–2113 | DOI: 10.2337/db12-1459

Decreased heart rate variability (HRV) is a major risk factor for sudden death and cardiovascular disease. We previously demonstrated that parasympathetic dysfunction in the heart of the Akita type 1 diabetic mouse was due to a decrease in the level of the sterol response element–binding protein (SREBP-1). Here we demonstrate that hyperactivity of glycogen synthase kinase-3β (GSK3β) in the atrium of the Akita mouse results in decreased SREBP-1, attenuation of parasympathetic modulation of heart rate, measured as a decrease in the high-frequency (HF) fraction of HRV in the presence of propranolol, and a decrease in expression of the G-protein coupled inward rectifying K^+ (GIRK4) subunit of the acetylcholine (ACh)-activated inward-rectifying K^+ channel (I_{KACh}), the ion channel that mediates the heart rate response to parasympathetic stimulation. Treatment of atrial myocytes with the GSK3β inhibitor Kenpaullone increased levels of SREBP-1 and expression of GIRK4 and I_{KACh}, whereas a dominant-active GSK3β mutant decreased SREBP-1 and GIRK4 expression. In Akita mice treated with GSK3β inhibitors Li^+ and/or CHIR-99021, Li^+ increased I_{KACh}, and Li^+ and CHIR-99021 both partially reversed the decrease in HF fraction while increasing GIRK4 and SREBP-1 expression. These data support the conclusion that increased GSK3β activity in the type 1 diabetic heart plays a critical role in parasympathetic dysfunction through an effect on SREBP-1, supporting GSK3β as a new therapeutic target for diabetic autonomic neuropathy.

Diabetic autonomic neuropathy (DAN) is a major complication of diabetes and has been associated with a marked increase in the incidence of sudden death in patients with diabetes (1,2). Risk factors for sudden death include clinical manifestations of parasympathetic dysfunction such as a decreased high-frequency (HF) component of heart rate variability (HRV) and increased dispersion of QT intervals (2–4). Fifty percent of patients with diabetes for 10 years or more have an impaired response of the heart to parasympathetic stimulation, characterized by a reduction in the HF component of HRV (5). Studies of type 1 diabetic patients who die suddenly in their sleep, "dead in bed syndrome," suggested that HRV analysis of diabetic patients who lack clinical evidence of autonomic neuropathy often demonstrate decreased parasympathetic tone (6). Hence, decreased HRV is an important risk factor for arrhythmia and sudden death in patients with diabetes.

Parasympathetic modulation of heart rate is mediated by binding of acetylcholine (ACh) released in response to vagal stimulation to M^2 muscarinic receptors resulting in hyperpolarization of the myocyte membrane and prolonged diastolic depolarization through the ACh-activated

[1]Molecular Cardiology Research Institute, Tufts Medical Center, Boston, MA
[2]Departments of Neurology and Physiology, Medical College of Wisconsin, Milwaukee, WI
[3]Department of Medicine, Tufts University School of Medicine, Boston, MA
[4]Department of Neuroscience, Tufts University School of Medicine, Boston, MA
[5]Stanley Center for Psychiatric Research, Broad Institute of Harvard and Massachusetts Institute of Technology, Cambridge, MA
[6]Department of Biochemistry & Molecular Biology, Louisiana State University School of Medicine, New Orleans, LA

Corresponding authors: Jonas B. Galper, jgalper@tuftsmedicalcenter.org, and Ho-Jin Park, hpark@tuftsmedicalcenter.org.

Received 24 October 2012 and accepted 14 January 2014.

This article contains Supplementary Data online at http://diabetes.diabetesjournals.org/lookup/suppl/doi:10.2337/db12-1459/-/DC1.

Y.Z. and C.M.W. contributed equally to this work.

See accompanying article, p. 1847.

inward-rectifying K^+ channels (I_{KACh}) located primarily in the atria. I_{KACh} is a heterotetrameric G-protein coupled inward rectifying K^+ channel (GIRK) composed of $(GIRK1)_2$/$(GIRK4)_2$ subunits, activated in response to the binding of the βγ-subunit of the heterotrimeric G-protein, G_{i2}, which is released after the binding of ACh to the M_2 muscarinic receptor (7,8). The GIRK4 subunit is essential for the formation of functional channels (9) and may regulate the expression of GIRK1 while protecting GIRK1 from proteolytic degradation. Thomas et al. (10) demonstrated that treatment of chick embryonic atrial myocytes with muscarinic agonists decreased levels of GIRK1 and GIRK4 proteins and mRNAs. RFamide-related peptides induced an outward current in *Xenopus* oocytes that depended on the expression of GIRK1 and GIRK4 and associated with pain in the rat (11). Most interestingly, chronic atrial fibrillation in humans has been associated with the downregulation of GIRK4, I_{KACh}, and decreased muscarinic receptor–mediated shortening of the action potential duration (12). However, none of these studies directly addressed the mechanism of regulation of GIRK4 expression.

Sterol regulatory element–binding proteins (SREBPs) are lipid-sensitive transcription factors that regulate the expression of enzymes involved in cholesterol metabolism, fatty acid synthesis, and glycolysis (13–15). We have demonstrated that SREBP-1 upregulates the expression of $G\alpha_{i2}$ and GIRK1 in atrial myocytes and also the negative chronotropic response of the heart to the ACh analog carbamylcholine (16,17).

The Akita type 1 diabetic mouse is characterized by a point mutation in the proinsulin *ins2* (*Ins2*^{Cys96Tyr}) gene that interferes with insulin processing and results in the destruction of pancreatic β-cells and the development of the diabetic phenotype (18) and secondary effects of diabetes (19). We recently demonstrated that the hypoinsulinemia in the Akita mouse is associated with a decrease in the response of the heart rate to carbamylcholine and decreased expression of SREBP-1 and GIRK1 (20), supporting the conclusion that insulin might regulate the parasympathetic response and I_{KACh} by the control of SREBP-1.

Glycogen synthase kinase (GSK) 3β is a serine/threonine kinase originally identified as an enzyme that phosphorylates and downregulates glycogen synthase (21). GSK3β is highly active in the basal state and is inactivated by phosphorylation at the regulatory Ser9 residue in response to insulin stimulation of the insulin receptor/insulin receptor substrate/phosphatidyl inositol 3-kinase (PI3K)/Akt cascade (22) (outlined in Fig. 1*A*). Insulin deficiency results in decreased phosphorylation and hyperactivity of GSK3β and has been implicated in diabetic nephropathy and/or retinopathy (23). This study used inhibitors of specific steps in the insulin cascade as well as inhibitors of GSK3β activity, with the goals of determining whether increased GSK3β activity in the Akita mouse heart plays a unique role in regulating the autonomic response of the heart via the regulation of SREBP-1 (Fig. 1*A*) and, hence, might serve as a new therapeutic target for the treatment of DAN.

RESEARCH DESIGN AND METHODS

Materials and Animals

Akita type 1 diabetic mice (C57BL/6-Ins2^{Akita}/J) were obtained from The Jackson Laboratory, Bar Harbor, ME. Adenovirus green fluorescent protein (Ad-GFP)–dominant-negative (DN)–SREBP-1 was a gift from Dr. Bruce Spiegelman, Dana Farber Cancer Institute and Harvard Medical School, Boston, MA. Ad-GFP-βgal was a gift from Dr. Anthony Rosenzweig, Beth Israel Deaconess Hospital and Harvard Medical School, Boston, MA. The dominant-active (DA)–GSK3β (S9A)-expressing adenovirus was provided by Dr. Thomas Force, Jefferson Heart Institute, Philadelphia, PA. The GIRK4-specific antibody for mouse was from Santa Cruz Biotechnology and a custom antibody generated by Chi Scientific (Maynard, MA). The peptide antigen was KKPRQRYMEKSGKC from the N-terminal region (34–47) of chick GIRK4 (National Center for Biotechnology Information accession #AAB95313). SREBP-1 and β-actin antibody were from Santa Cruz Biotechnology. β-Catenin, phosphorylated (p)-Akt (Ser473), Akt, p-GSK3β (Ser9), and GSK3β were from Cell Signaling Technology, Beverly, MA. The PI3K inhibitor LY294002 and the GSK3β inhibitor Kenpaullone were from Calbiochem. CHIR-99021 was a gift from the Broad Institute, Cambridge, MA. The heterozygous male diabetic Akita *Ins2*^{Cys96Tyr} mice and littermate wild-type (WT) mice were from The Jackson Laboratory.

To monitor the progression of disease, measurements of urine glucose, protein, and ketones were made with Keto-Diastix Reagent Strips for Urinalysis (Bayer). Glucose was monitored using an Accu-Chek glucometer. Body weight and serum glucose levels are summarized in Supplementary Table 1. Akita mice demonstrated decreased body weight and marked hyperglycemia compared with WT mice. Insulin pellets releasing 0.1 units/implant/day or placebo pellets (Linshin Canada Inc., Toronto, ON, Canada) were implanted subcutaneously. Serum glucose was monitored daily until stabilized, 10 days, and the number of pellets adjusted to maintain blood glucose levels at 100–150 mg/dL, as described previously (20). For Li^+ experiments, mice were fed normal chow or a diet supplemented with 0.2% LiCl (Harlan Laboratories) for 7 days. Serum levels of Li^+ in mice fed this diet have been shown to approximate those in patients receiving Li^+ therapy (24). All vertebrate animal-related procedures described here were approved by the Tufts Medical Center Institutional Animal Care Committee.

Electrocardiographic Monitoring, Heart Rate, and HRV Analysis in Conscious, Unrestrained Mice

Anesthesia was induced with inhaled 1.5% isoflurane in oxygen. An electrocardiogram (ECG) signal wireless radiofrequency transmitter was implanted in a subcutaneous

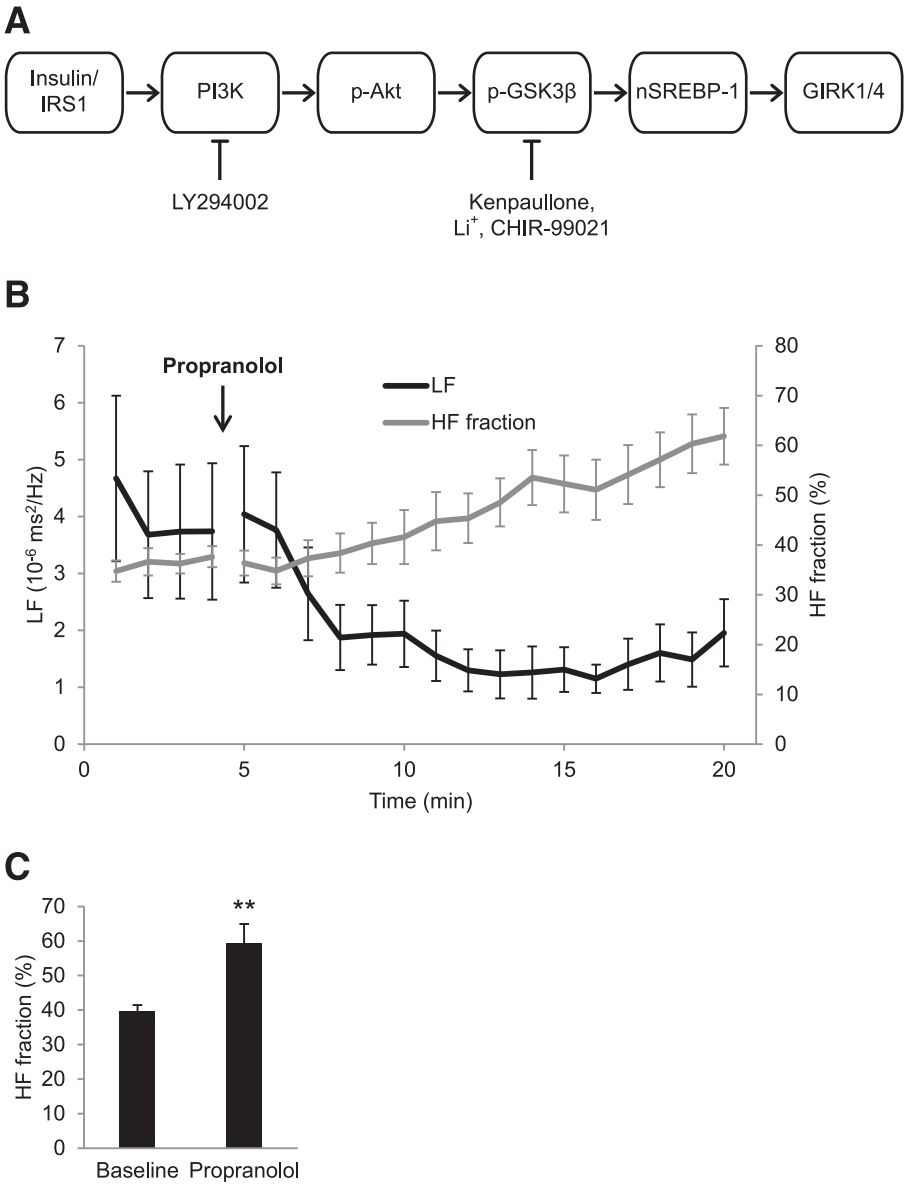

Figure 1—*A*: Schematic representation of the insulin-signaling cascade. Insulin binding to the insulin receptor results in phosphorylation of insulin receptor substrate (IRS1/2), which in turn activates PI3K, which converts Akt to the activated phosphorylated form. p-Akt phosphorylates and inactivates GSK3β, whose role in regulation of SREBP-1 and GIRK4 is suggested. LY294002 is a PI3K inhibitor; Kenpaullone, Li^+, and CHIR-99021 are GSK3β inhibitors. *B*: Time course of changes in HF fraction and the LF power in response to propranolol. ECGs were monitored in 4-month-old WT male mice and recorded continuously for 5 min before an intraperitoneal injection of 1 mg/kg propranolol and continued for 15 min. Composite plots of HF fraction and LF power were computed as described in RESEARCH DESIGN AND METHODS. *C*: Quantitation of HF fraction at baseline and 15 min after propranolol. Results are the mean ± SEM. $^{**}P < 0.01$.

pocket, and electrodes were sutured over the right pectoralis muscle and the lower left ribs in WT and Akita mice. The data were recorded at a sample rate of 5,000 Hz with the use of a telemetry receiver and an analog-to-digital acquisition system (Data Sciences International). The ECG signal was analyzed using custom-built software. Beat-to-beat heart rate data were computed and artifacts and nonsinus rhythms were removed after manual review. Composite heart rate plots and average heart rates and duration of bradycardia were computed as described precviously (17).

For HRV analysis, R wave detection and beat annotation were manually reviewed as above. All ectopic and postectopic beats and artifacts were removed and replaced with intervals interpolated from adjacent normal beats, discarding segments where gaps accounted for more than 15% of the recording segment. Frequency-domain analysis was performed after construction of an instantaneous RR-interval time series by resampling at 10 Hz.

The power spectra of detrended 2-min segments were computed for the frequency ranges of 0.5 to 1.5 Hz, designated as low-frequency (LF) power, and of 1.5 to 5 Hz,

designated as high-frequency (HF) power, as described previously (25,26). HF fraction was computed as HF/(LF + HF). The HF power has been shown to result predominantly from parasympathetic modulation of heart rate, whereas LF power has been shown to result from sympathetic as well as parasympathetic modulation of heart rate (27). To minimize the effects of activity of the mice, we chose segments in which the heart rate and frequency domain parameters were relatively stationary, verified by using Kalman-smoothing and wavelet-based visualization in addition to Fast Fourier transform (FFT)–derived spectrograms, and where noise caused by mouse movement and the associated muscle activity and changes in entropy were minimal.

We have developed a unique method for assessing parasympathetic modulation of the heart rate in our mouse model because we found the usual approach of administering atropine difficult in the presence of high baseline heart rates. To observe the parasympathetic influence on heart rate, we inhibited the sympathetic modulation of the heart rate. Specifically, given that inhibition of the β-adrenergic receptor blocks the sympathetic component of HRV, leaving the parasympathetic component relatively unopposed, we injected mice with the β-adrenergic receptor–blocker propranolol and computed the time course of the increase in the HF fraction. Composite plots of the HF fraction were computed from FFT power spectra over a 3-min sliding window of RR-interval data, repeated every 10 s and averaged to one HF fraction data point per minute per group (± SEM). Data outlined in Fig. 1*B* demonstrate that in response to propranolol, the HF fraction increases with a time course similar to that for the decrease in LF power.

For statistical comparisons between the groups, heart rate and frequency domain HRV parameters were computed for 2-min segments at the end of the baseline and propranolol phases. HF fraction increased from a mean of 39.65 ± 1.8% to 59.3 ± 5.6% (n = 13, P = 0.008; Fig. 1*C*), LF power decreased from 4.58 ± 1.01 to 2.49 ± 1.17 10^{-6} ms^2/Hz (P = 0.074), and HF power was relatively unchanged at 2.17 ± 0.57 and 1.81 ± 0.70 10^{-6} ms^2/Hz, respectively (P = 0.431; data not shown). These findings support the conclusion that the increase in HF fraction in response to propranolol is due primarily to a decrease in LF power. Absolute values for HF and LF for each study are given in Supplementary Table 3. Owing to the large variability of the absolute values of HF and LF between individual mice and treatment groups, we used the normalized HF parameter computed as HF fraction = HF/(HF + LF) (27). Hence, the HF fraction measurements after administration of propranolol reflect the parasympathetic component of HRV in the presence of sympathetic blockade. In these studies we compare differences in HF fraction after propranolol to assess parasympathetic dysfunction in a mouse model for type 1 diabetes.

Cell Culture, Adult Mouse Atrial Myocytes

Atrial myocytes from chick embryos 14 days in ovo were prepared by a modification of the method of DeHaan (28) as described previously (29). Dissociated atrial myocytes from mouse atria were prepared by a retrograde Langendorff perfusion method as described (20), with some modifications. Cells were rod shaped with clearly defined striations.

Adenoviral Infection

On the second culture day, cells had reached ~70% confluence and were infected with adenovirus at the indicated multiplicity of infection. After 2 days in culture, cells were harvested and whole-cell extracts were used for Western blot analysis, as outlined below.

Western Blot Analysis

To determine levels of gene expression in cultured atrial myocytes, cells were harvested, and Western blot analysis was done as described previously (17,30). Western blot analysis of expression of proteins in atria of WT and Akita diabetic mice was done on atrial homogenates. Protein concentration was determined by Bradford reagent (Bio-Rad). Each sample represents tissue from the atria of a single mouse.

Cellular Electrophysiology

Membrane currents were measured by the patch-clamp technique in whole-cell mode using an LM-EPC7 amplifier, as described (20). To obtain and maintain good seal formation required for membrane current recording, we found it necessary to suppress contraction with high external K^+ and 0 external Ca^{2+}, which leads to persistent membrane depolarization and inactivation of voltage-activated Na^+ channels. Neither condition has an effect on I_{KACh} (17). Whole-cell currents were elicited at room temperature in the presence and absence of 10 μmol/L carbamylcholine introduced by focal perfusion over 10–15 s, followed by washout. Currents returned to baseline within 10–15 s of washout. Currents were normalized to the cell capacitance determined by capacitance compensation, and data are presented as current density in pA/pF. Current-voltage (I-V) plots were constructed from a series of data points obtained from the carbamylcholine current responses at given voltages.

Echocardiography

Echocardiographic studies were performed as previously described (17). Briefly, the Sonos 7500 echocardiography system (Phillips Medical Systems) was used with a dynamically focused linear array transducer (15-6L Intraoperative Linear Array, Phillips Medical Systems) using a depth setting of 0.5–1.0 cm. Anesthesia was induced with inhaled 1.5% isoflurane in oxygen and maintained with inhaled 1.0% isoflurane in oxygen. Animals were placed on a warming pad to maintain body temperature at 36.5°–37.5°C.

Statistics

All values are expressed as mean ± SEM. Statistical differences between mean values were calculated by independent or pairwise Student t test, as appropriate. Normal

distribution assumptions were verified using the Shapiro-Wilk test. A P value of < 0.05 was considered significant.

RESULTS

Decreased HRV in the Type 1 Diabetic Akita Mouse

We previously reported that the negative chronotropic response to carbamylcholine in Akita mice was markedly blunted compared with WT mice and that these effects were reversed by insulin treatment (20). To establish the clinical significance of these findings and their relevance as a cardiovascular risk factor, we determined whether the parasympathetic modulation of heart rate was also decreased in the type 1 diabetic Akita mouse compared with the WT mouse. Given that inhibition of the β-adrenergic receptor blocks the sympathetic component of HRV, leaving the parasympathetic component relatively unopposed, we compared the time course of the increase in HF fraction after the injection of the β-adrenergic receptor blocker propranolol in Akita and WT mice (described in RESEARCH DESIGN AND METHODS and Fig. 1*B*). The composite plot of the HF fraction in WT mice increased continually during the time period studied, whereas the HF fraction in the Akita mouse reached a plateau 10 min after the propranolol injection (Fig. 2*A*). At 15 min after the propranolol injection, the 2-min mean of HF fraction was significantly higher in WT mice, 70.9 ± 4.8%, compared with 48.6 ± 5.2% in Akita mice (n = 10, P = 0.005; Fig. 2*B*).

For further validation of these findings, we treated WT and Akita mice with atropine, because the increase in heart rate in response to muscarinic blockade by atropine also reflects the level of parasympathetic stimulation of the heart. Heart rate was measured for 3 min before and after injection with atropine (0.5 mg/kg). The mean heart rate in WT mice increased by 185.1 ± 25.9 bpm and by 98.1 ± 7.0 bpm in Akita mice (n = 9, P = 0.01; Fig. 2*C*), consistent with the increase in the HF fraction after propranolol. Furthermore, to determine whether the observed differences in the HF fraction between Akita and WT mice might be influenced by differences in sympathetic input to the heart, we compared the decrease in the WT and Akita mice heart rate for 15 min after the propranolol injection. The heart rate decreased by 65.8 ± 22.5 bpm in WT mice and by 79.1 ± 22.6 bpm in Akita mice (n = 10, P = 0.628; Supplementary Table 4). Finally, the baseline HF fraction measured before the propranolol injection was not significantly different in the two groups, at 34.5 ± 2.3% versus 37.2 ± 2.4%, respectively (n = 10, not significant; data not shown).

To determine whether the abnormality of HRV in the Akita mouse was due to hypoinsulinemia, we compared the time course of the effect of the propranolol injection on the HF fraction before and after implantation of slow-release insulin pellets. After insulin treatment, HF fraction increased over time, with a brief plateau 8 min after the propranolol injection, similar to that seen in Akita mice before insulin treatment. However, unlike untreated Akita mice, after reaching this plateau, the HF fraction in insulin-treated mice continued to increase over time (Fig. 2*D*). At 15 min after the propranolol injection, the 2-min average HF fraction was significantly higher, at 75.2 ± 4.6% postinsulin, compared with 51.5 ± 3.0% preinsulin (n = 8, P = 0.004; Fig. 2*E*). There was no significant difference in the decrease in mean heart rate in response to propranolol in Akita mice before and after insulin treatment, consistent with the conclusion that insulin had no effect on the sympathetic response of the heart (see Supplementary Table 4). Baseline HF fraction was not significantly different before and after insulin treatment (38.6 ± 4.0% vs. 42.0 ± 3.4%, n = 8, not significant; data not shown). These data are consistent with the conclusion that parasympathetic modulation of the heart rate in the Akita mouse was impaired secondary to hypoinsulinemia.

Decreased HRV in Akita Diabetic Mice Is Associated With Decreased Expression of GIRK4 and Decreased Insulin Signaling

Although GIRK4 expression in the atrium has been shown to be altered in the presence of atrial fibrillation (12), mechanisms of regulation of GIRK4 expression and their role in parasympathetic signaling have not been studied. To determine whether decreased expression of GIRK4 might be associated with the decreased HRV in the Akita mouse, we compared levels of GIRK4 expression in the atria of WT and Akita mice. Data in Fig. 3*A* demonstrate that GIRK4 expression in the atria of Akita mice was decreased 0.54 ± 0.07-fold compared with WT mice (n = 14, P = 0.00002). To determine if this effect was due to decreased insulin levels in the Akita mouse, Akita mice were treated for 10 days with placebo or slow-release insulin pellets. After 2 days, glucose levels in insulin-treated mice reached those in WT mice (Supplementary Table 1). Data summarized in Fig. 3*B* demonstrate that GIRK4 expression in the atria of placebo-treated Akita mice was 0.46 ± 0.07-fold lower than in WT mice (1.00 ± 0.07-fold; n = 5, P = 0.0003). Insulin treatment resulted in an increase from 0.46 ± 0.07-fold to 0.94 ± 0.05-fold (n = 6, P = 0.0002). To identify downstream kinases in the insulin-signaling pathway that might be involved in the regulation of GIRK4 expression and the associated decrease in HRV and heart rate response in Akita mice (see pathway outlined in Fig. 1*A*), the levels of p-Akt and p-GSK3β in atria of WT and placebo-treated Akita mice were compared. Levels of p-Akt and p-GSK3β were decreased 0.62 ± 0.06-fold (n = 11, P = 0.004) and 0.38 ± 0.06-fold (n = 8, P = 0.0003), respectively, in the atria of Akita mice compared with 1.0 ± 0.11-fold in the atria of WT mice (n = 8; Fig. 3*C* and *D*). Insulin treatment stimulated p-Akt levels from 0.62 ± 0.06- to 1.95 ± 0.38-fold (P = 0.005) and p-GSK3β levels from 0.38 ± 0.06- to 0.68 ± 0.08-fold (P = 0.007).

Insulin Regulates the Expression of GIRK4 by PI3K/Akt

Because obtaining mouse atrial myocytes in sufficient quantities for Western blot analysis was not possible,

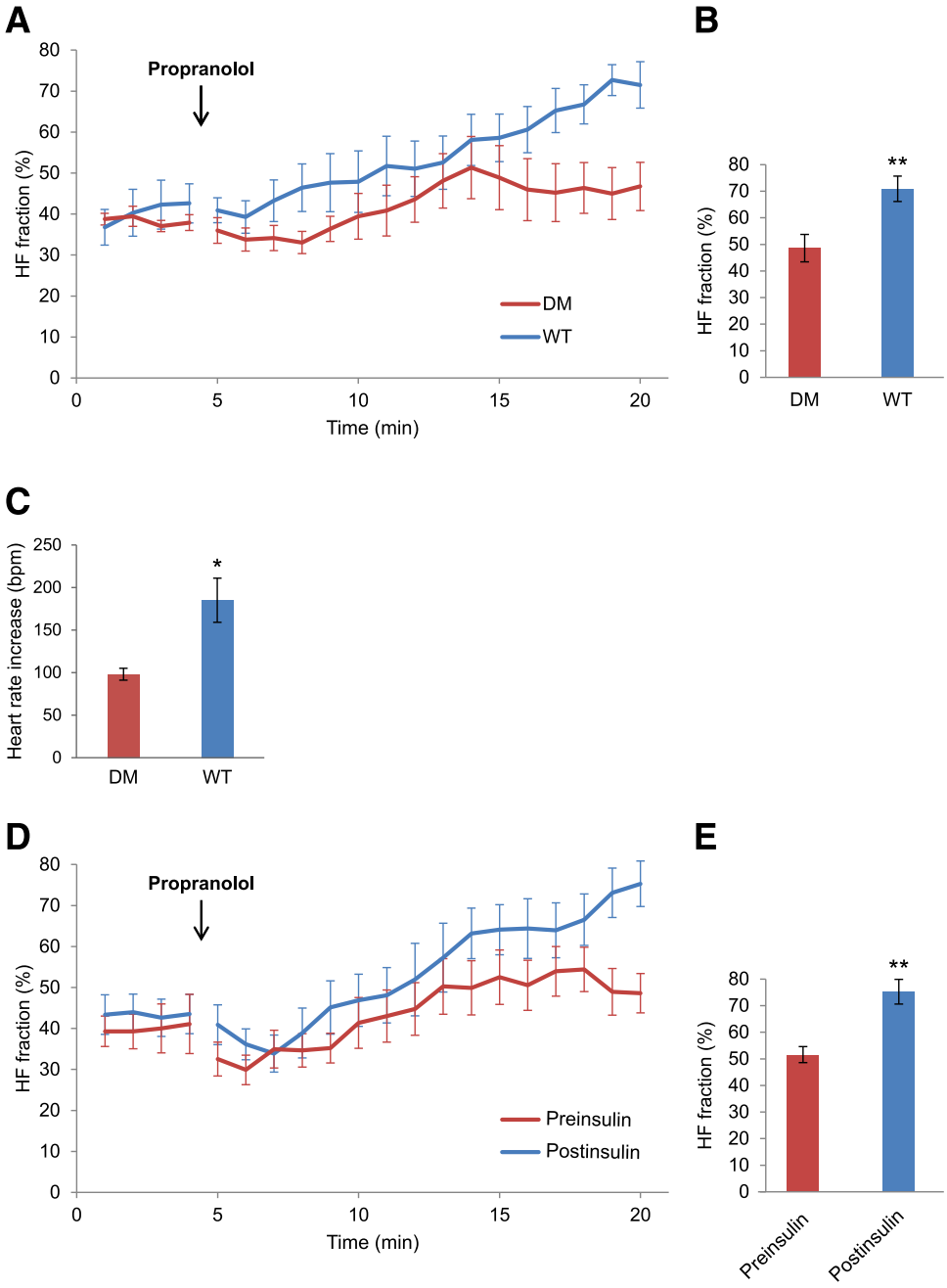

Figure 2—Comparison of HF fraction of HRV in WT, Akita, and insulin-treated Akita mice, as well as heart rate change after atropine injection in WT and Akita mice. ECGs were monitored in 4-month-old male mice before the intraperitoneal injection of 1 mg/kg propranolol and continued for 15 min as described in RESEARCH DESIGN AND METHODS. *A*: Comparison of groupwise averaged (± SEM) composite plots of the HF fraction before and over the duration of the propranolol phase in WT and Akita diabetic mice (DM). *B*: Quantitation of HF fraction at 15 min after propranolol injection. *C*: Comparison of the increase in heart rate averaged for 3 min before and 3 min after the injection of atropine in Akita and WT mice. *D*: Comparison of composite plots of the response of Akita mice to propranolol before (preinsulin) and 10 days after insulin treatment (postinsulin). Each mouse served as its own control. *E*: Quantitation of HF fraction at 15 min after propranolol injection before and after insulin treatment. Results are reported as mean ± SEM. Statistical comparisons were by Student *t* test throughout the figure. $^{*}P < 0.05$, $^{**}P < 0.01$.

cultured embryonic chick atrial myocytes were used to determine the role of insulin signaling in the control of GIRK4 expression. Insulin treatment of embryonic atrial myocytes increased the GIRK4 protein level 1.72 ± 0.19-fold (n = 12, P = 0.003) compared with control myocytes in parallel with increased phosphorylation of Akt and GSK3β (Fig. 4*A* and *B*), consistent with the effects of insulin treatment on GIRK4 in the atria of Akita mice (Fig. 3). Treatment of atrial myocytes with the PI3K inhibitor LY294002 reversed insulin stimulation of GIRK4

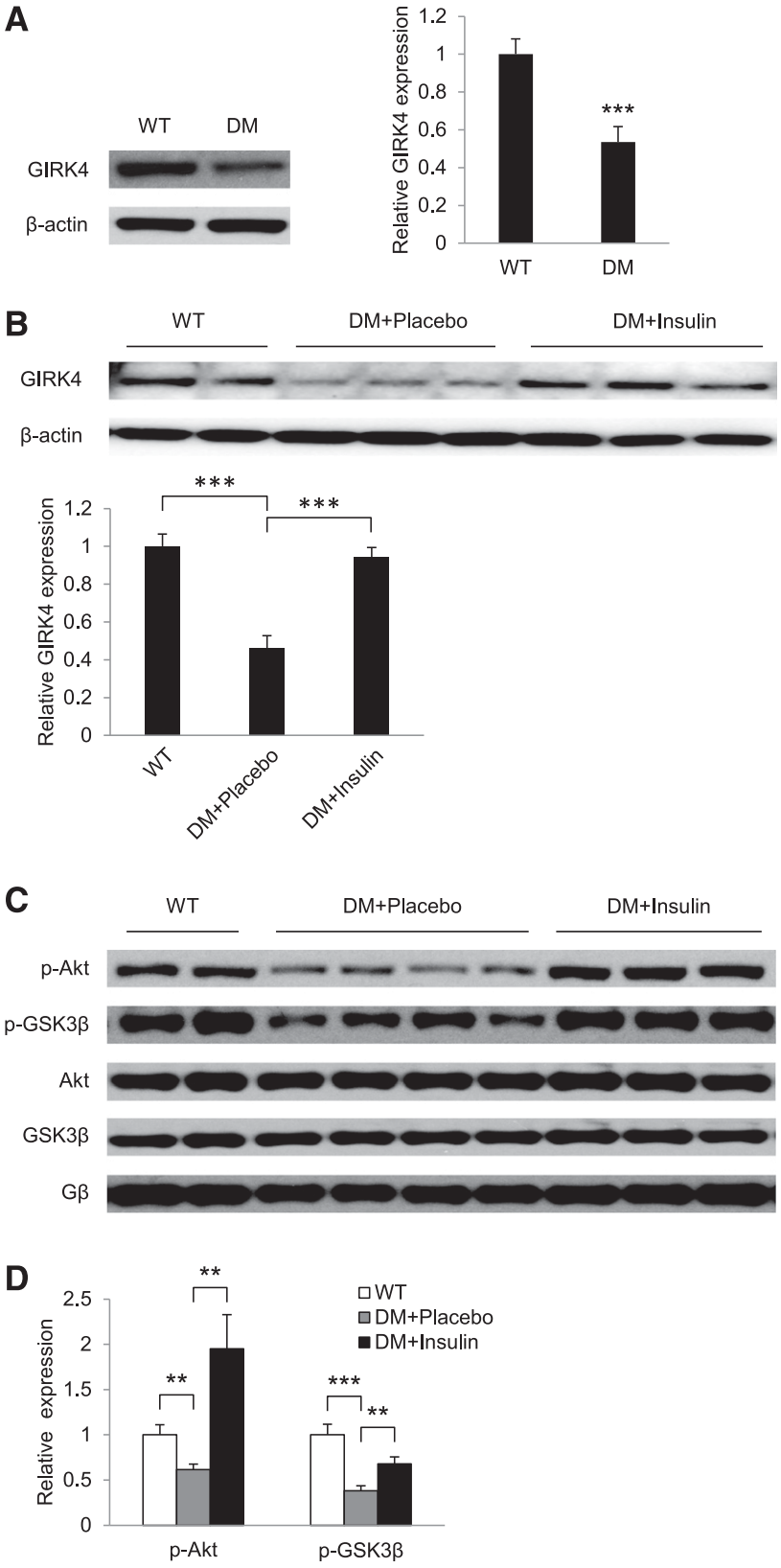

Figure 3—GIRK4 expression and insulin signaling are decreased in atria of Akita diabetic mice (DM). Western blot analysis of GIRK4 expression in atria of WT and Akita (DM) mice (*A*) and WT mice and placebo- and insulin-treated Akita mice (*B*). The bar graphs represent densitometry analysis of Western blots normalized to β-actin. *C*: Western blot analysis of p-Akt, Akt, p-GSK3β, and GSK3β in atria of age-matched WT and placebo- and insulin-treated Akita mice. *D:* Bar graphs of levels of p-Akt and p-GSK3β in placebo (DM+Placebo) and insulin-treated Akita mice normalized to the expression of the β subunit of $G\alpha_{i2}$. $^{**}P < 0.01$, $^{***}P < 0.001$.

expression and inhibited insulin stimulation of p-Akt and p-GSK3β (Fig. 4*A* and *B*), consistent with the conclusion that insulin regulation of the expression of GIRK4 depends on the activation of the PI3K/Akt/GSK3β pathway (Fig. 1*A*).

Insulin Regulation of GIRK4 in Atrial Myocytes Depends on SREBP-1

We previously demonstrated that parasympathetic dysfunction in the type 1 diabetic Akita mouse is associated with an insulin-dependent decrease in levels of SREBP-1 in the atrium of the Akita mouse (20). To determine whether SREBP-1 played a role in insulin regulation of GIRK4 expression, we used cultured chick atrial myocytes. First, we determined the role of PI3K on levels of SREBP-1 and the role of SREBP-1 in GIRK4 expression. Insulin treatment of chick atrial myocytes increased the expression of the 60-kDa nuclear form of SREBP-1 (nSREBP-1) 1.65 ± 0.11-fold (n = 6, P = 0.0003) compared with control cells. The PI3K inhibitor LY294002 completely reversed this effect (Fig. 4*A* and *B*), consistent with the conclusion that insulin regulation of SREBP-1 depends on the activation of PI3K. To determine whether the PI3K-dependent increase in nSREBP-1 in response to insulin might play a role in the insulin regulation of GIRK4 expression demonstrated in Fig. 3*B* and in Fig. 4*A* and *B*, chick atrial myocytes were infected with an adenovirus expressing Ad-GFP or DN–SREBP-1 (Ad-GFP–DN–SREBP-1), followed by incubation for 16 h with insulin. Fluorescence microscopy demonstrated that GFP was expressed in 90% of atrial myocytes infected with Ad-GFP (17,20). Insulin treatment of cells infected with Ad-GFP increased GIRK4 expression 1.52 ± 0.13-fold (n = 8, P = 0.006) compared with control cells. Insulin treatment of cells infected with Ad-GFP–DN–SREBP-1 resulted in a decreased GIRK4 expression (0.75 ± 0.11-fold) compared with cells treated with Ad-GFP (n = 8, P = 0.006; Fig. 4*C* and *D*). Taken together, these data support the conclusion that insulin stimulation of GIRK4 expression in atrial myocytes depends on SREBP-1 through the PI3K/Akt pathway.

GSK3β Regulates the Level of SREBP-1 and the Expression of GIRK4

Data presented in Fig. 3*C* and *D* demonstrated that pGSK3β was markedly decreased in the atrium of Akita mice compared with WT mice and that insulin reversed this effect. Hence, GSK3β activity is markedly increased

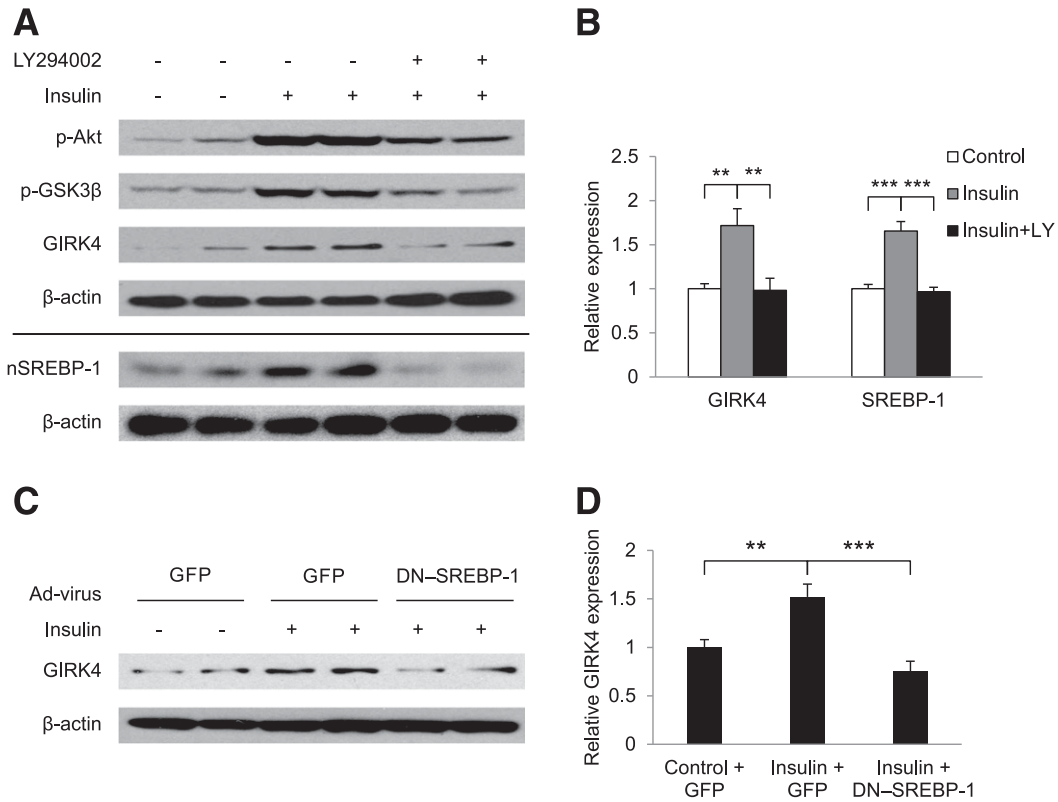

Figure 4—Insulin stimulation of GIRK4 expression depends on PI3K and SREBP-1. Embryonic chick atrial myocytes were incubated for 16 h with vehicle or 100 nmol/L insulin, with or without 10 μmol/L LY294002. *A*: Effect of LY294002 on expression of GIRK4, p-Akt, p-GSK3β, and nSREBP-1 as determined by Western blot analysis. *B*: Densitometric analysis of GIRK4 and nSREBP-1 expression from experiments similar to those in panel *A* normalized to β-actin. *C*: Effect of infection of embryonic chick atrial myocytes with Ad-GFP or GFP–DN–SREBP-1 on insulin-stimulated GIRK4 expression. *D*: Densitometric analysis of GIRK4 expression from experiments similar to those in *panel C* normalized to β-actin. $^{**}P < 0.01$, $^{***}P < 0.001$.

in atria of Akita mice. Furthermore, insulin stimulation of GIRK4 expression and nSREBP-1 levels in chick atrial myocytes was associated with a marked increase in p-GSK3β (Fig. 4*A* and *B*), which was inhibited by LY294002. Given that insulin inactivates GSK3β by a PI3K/Akt-dependent pathway, we used chick atrial myocytes to determine the effect of inhibition of GSK3β on insulin regulation of SREBP-1 levels and GIRK4 expression. Cells were treated with increasing doses of Kenpaullone, a competitive GSK3β inhibitor that binds to the ATP binding site of GSK3β (31). Incubation with Kenpaullone for 24 h increased nSREBP-1 and the expression of GIRK4 in a dose-dependent manner (Fig. 5*A* and *B*) at concentrations of Kenpaullone that are selective for GSK3β inhibition (31). Compared with control, Kenpaullone increased GIRK4 1.69 ± 0.18-fold (n = 5, P = 0.018) at 2 μmol/L and 3.09 ± 0.35-fold (n = 7, P = 0.011) at 5 μmol/L, whereas nSREBP-1 increased 3.21 ± 0.58-fold (n = 6, P = 0.033) at 5 μmol/L Kenpaullone. Furthermore, Kenpaullone increased levels of β-catenin in a dose dependent-manner consistent with its inhibitory effect on GSK3β activity (Fig. 5*A*). Given that Kenpaullone inhibits GSK3α and GSK3β, we determined the effect of adenoviral expression of an HA-tagged DA-GSK3β (S9A) mutant on GIRK4 and SREBP-1 levels in atrial myocytes (32). Western blot analysis demonstrated that in chick atrial myocytes infected with HA-DA-GSK3β, GSK3β migrated as a doublet, consistent with expression of the more slowly migrating HA-tagged form. Overexpression of DA-GSK3β decreased the levels of nSREBP-1, GIRK4, and β-catenin expression in a dose-dependent manner (Fig. 5*C* and *D*). These results suggest that GSK3β is a negative regulator for SREBP-1 and GIRK4 and are consistent with the hypothesis that increased GSK3β activity due to decreased insulin levels might result in decreased SREBP-1–dependent GIRK4 expression.

Overexpression of a Constitutively Activated Akt (Myristoylated Akt) in Atrial Myocytes Mimics the Effect of Insulin on GSK3β, nSREBP-1, and GIRK4

To further delineate the role of the PI3K/Akt/GSK3β pathway in insulin regulation of SREBP-1–dependent expression of GIRK4, atrial myocytes were infected with an adenovirus expressing the activated myristoylated form of Akt (Myr-Akt) or a control vector expressing Ad-GFP. Expression of Myr-Akt resulted in an increase in the phosphorylation of GSK3β (Fig. 5*E*), a 1.71 ± 0.18-fold (n = 10, P = 0.003) increase in nSREBP-1, and a 3.88 ± 0.55-fold (n = 6, P = 0.003) increase in GIRK4 expression compared with cells infected with a vector expressing Ad-GFP alone (Fig. 5*E* and *F*).

Inhibition of GSK3β Increases I_{KACh} in HL-1 Cells

To determine the physiological relevance of GSK3β regulation of GIRK4 expression in atrial myocytes (Fig. 5), we determined the effect of the inhibition of GSK3β activity on the response of I_{KACh} to parasympathetic stimulation in HL-1 cells, an immortalized mouse atrial myocyte line. HL-1 cells have been shown to demonstrate contractile, morphologic, biochemical, and electrophysiological properties characteristic of atrial myocytes (33). To establish the presence of the insulin-signaling pathway in these cells, they were treated with insulin, and the phosphorylation of downstream kinases was determined. Insulin treatment and expression of Myr-Akt resulted in increases in p-Akt, p-GSK3β, nSREBP-1, and in the expression of GIRK4 (Supplementary Fig. 1*a* and *b*). Finally, treatment of HL-1 cells with Kenpaullone increased the levels of nSREBP-1 and GIRK4 (Supplementary Fig. 1*c*), consistent with the conclusion that HL-1 cells were an appropriate model for the study of insulin regulation of GIRK4 expression by an Akt/GSK3β-dependent pathway.

To determine whether GSK3β played a role in the regulation of I_{KACh}, we compared membrane currents from HL-1 cells cultured with vehicle or Kenpaullone (Supplementary Fig. 2). The current-voltage (I-V) relationships demonstrated inward rectification with a reversal potential at −28 mV consistent with a K^+-dependent current at 50 mmol/L extracellular K^+. The peak inward current increased from −22.4 ± 3.2 pA/pF in cells cultured in vehicle to −53.2 ± 5.8 pA/pF (n = 15, $P < 0.001$) in cells treated with Kenpaullone, with no change in reversal potential (Supplementary Fig. 2*b* and *c*).

Li^+ Treatment Reverses the Parasympathetic Dysfunction in the Akita Mouse

These data suggested that insulin regulates GIRK4 expression by an Akt/GSK3β-dependent pathway and that GSK3β regulates I_{KACh} in HL-1 cells. To determine whether the decrease in the HF fraction in the Akita mouse described in Fig. 2 and the impaired heart rate response of the Akita mouse to carbamylcholine described previously (20) might be associated with increased GSK3β activity in the diabetic heart, male Akita mice, 4 months of age, were fed a diet containing Li^+, a GSK3β inhibitor, for 7 days.

The heart rate response to the ACh analog carbamylcholine was compared in mice before and 7 days after the initiation of Li^+ treatment. Mice were treated first with propranolol to block the reflex response, followed by carbamylcholine (Fig. 6*A*). Li^+ had no significant effect on the response of the heart rate to propranolol. However, the duration of bradycardia after carbamylcholine administration plotted here as heart rate plateau increased from 5.9 ± 0.6 min pre-Li^+ to 9.5 ± 1.5 min post-Li^+ (n = 11, $P < 0.05$; Fig. 6*A* and *B*, *left panel*). Furthermore, the absolute decrease in the heart rate in response to carbamylcholine was increased from 244 ± 20 bpm pre-Li^+ to 304 ± 14 bpm (n = 11, $P < 0.05$) after Li^+ treatment (Fig. 6*A* and *B*, *right panel*). To determine the effect of Li^+ treatment on the HF fraction, we compared the time course of the increase in the HF fraction in response to the propranolol injection in Akita mice before and after Li^+ treatment. Composite plots of the HF fraction demonstrated that before Li^+ treatment, the HF

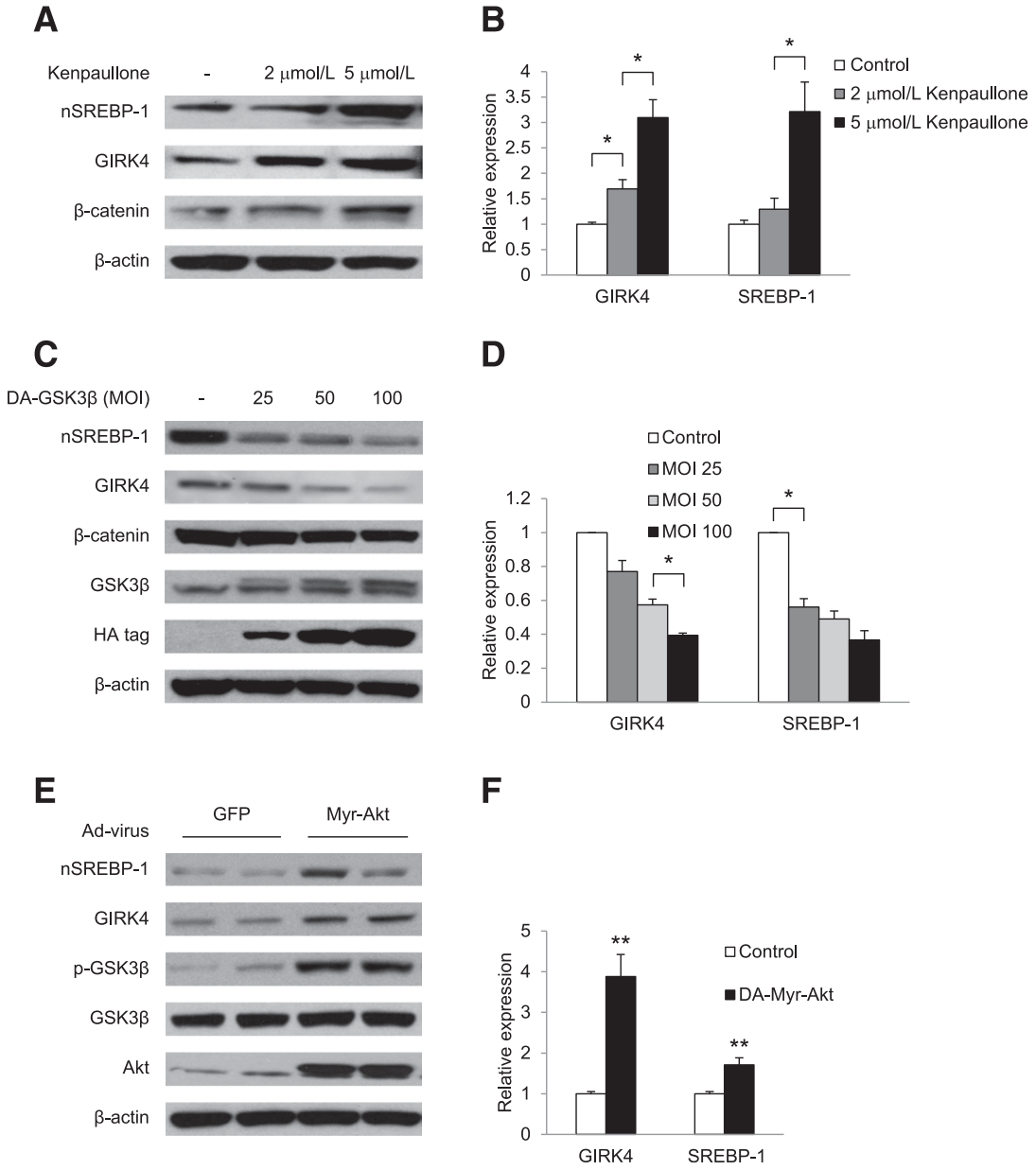

Figure 5—GSK3β regulation of nSREBP-1 and GIRK4 levels in chick atrial myocytes. *A*: Western blots demonstrate dose dependence of Kenpaullone inhibition of GSK3β on GIRK4 and nSREBP-1 levels. *B*: Densitometric analysis of Western blots similar to those in *A*, normalized to β-actin. *C*: Western blot analysis of levels of GIRK4 and nSREBP-1 protein in atrial myocytes infected with increasing multiplicity of infection (MOI) of an adenovirus expressing an HA-tagged DA-GSK3β. *D*: Densitometric analysis of Western blots similar to those in *C*. *E:* Effect of adenoviral expression of Myr-Akt on the phosphorylation of GSK3β and levels of nSREBP-1 and GIRK4 proteins. Chick atrial myocytes were infected with Ad-Myr-Akt or Ad-GFP at an MOI of 50 pfu/cell for 3 h, followed by incubation for 48 h in fresh medium. Cells were harvested, and levels of nSREBP-1, GIRK4, and p-GSK3β were determined. *F:* Densitometric analysis of Western blots similar to those in *E*. Data are normalized to β-actin. $^*P < 0.05$, $^{**}P < 0.01$.

fraction reached a plateau 8 min after the propranolol injection. After Li^+ treatment, the HF fraction also reached a relative plateau but continued to increase during a second phase (Fig. 6*C*). At 15 min after the propranolol injection, the 2-min mean of HF fraction increased from 50.6 ± 4.4% pre-Li^+ to 73.5 ± 3.2% (n = 10, $P < 0.001$) post-Li^+ (Fig. 6*D*). No significant difference was noted in the decrease in the mean heart rate in response to propranolol in Akita mice before and after Li^+ treatment, consistent with the conclusion that Li^+ had no effect on the sympathetic response of the heart (see Supplementary Table 4).

Echocardiographic analysis demonstrated that Li^+ had no effect on left ventricular end diastolic dimension, left ventricular end systolic dimension, fractional shortening, ejection fraction, or resting heart rate (see Supplementary Table 2). Hence, changes in autonomic response in Li^+-treated mice were not associated with changes in ventricular function.

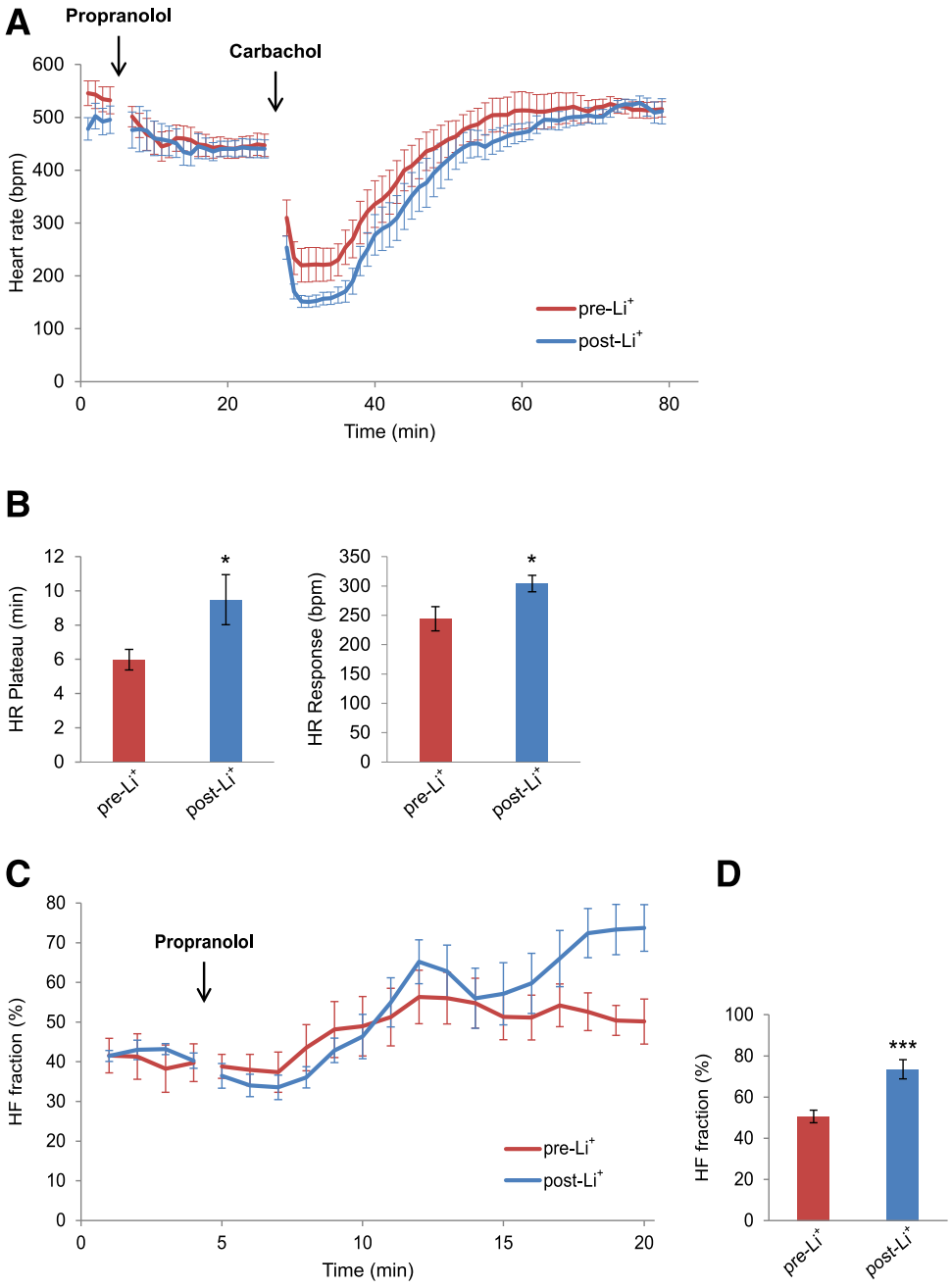

Figure 6—Li^+ treatment of the Akita mouse increases both the negative chronotropic response of the heart to the parasympathetic receptor agonist carbamylcholine and the HF fraction of HRV. *A*: Negative chronotropic response of 4-month-old male Akita mice to carbamylcholine before and after a 7-day treatment with Li^+. Mice were pretreated with intraperitoneal (i.p.) propranolol, 1 mg/kg, to block the β-adrenergic reflex response to carbamylcholine, followed 20 min later by 0.2 mg/kg i.p. carbamylcholine. Heart rate was recorded as described in RESEARCH DESIGN AND METHODS. Data are the composite mean heart rates obtained from moving average beat data of 11 Akita mice before Li^+ (pre-Li^+) and 7 days after Li^+ (post-Li^+). *B*, *Left panel*: Duration of bradycardia after carbamylcholine injection defined as the elapsed time from the carbamylcholine-induced bradycardia until the initiation of recovery given here as the heart rate plateau. *Right panel*: Magnitude of the negative chronotropic response to carbamylcholine. The difference between baseline heart rate immediately before carbamylcholine injection and the lowest heart rate after carbamylcholine injection were used to compute the heart rate response. *C*: Composite plots of the averaged (± SEM) time course of the increase in HF fraction after injection of propranolol in mice pre-Li^+ and post-Li^+. *D*: Comparison of the magnitude of HF fraction pre-Li^+ and post-Li^+ computed 15 min after propranolol injection. For these experiments, each mouse served as its own control. $^*P < 0.05$, $^{***}P < 0.01$

Li^+ Treatment Increases I_{KACh} in Atrial Myocytes From Akita Mice in Parallel With Increased nSREBP-1 Levels and GIRK4 Expression in the Atrium

To determine whether Li^+ might increase parasympathetic responsiveness in Akita mice by an effect on I_{KACh}, we measured I_{KACh} in atrial myocytes from untreated and Li^+-treated Akita mice. The carbamylcholine-stimulated peak inward current increased from -188.7 ± 15.4 pA/pF ($n = 12$) in atrial myocytes from untreated Akita mice to -370 ± 39.6 pA/pF ($n = 12$, $P = 0.006$) in atrial myocytes from Li^+-treated Akita mice (Fig. 7*A–C*). We had previously demonstrated a peak inward current of -451 ± 62 pA/pF in WT mice (20). Hence, Li^+ treatment partially reversed the abnormality in I_{KACh} in Akita mice. We further compared the levels of nSREBP-1 and GIRK4 in extracts of atria from WT and untreated and Li^+-treated Akita mice. Expression of nSREBP-1 and GIRK4 were 0.48 ± 0.14-fold ($n = 6$, $P = 0.014$) and 0.48 ± 0.09-fold ($n = 5$, $P = 0.003$), respectively, in Akita compared with WT atria (Fig. 7*D* and *E*), consistent with our prior observations (20) and data summarized in Fig. 3. However, Li^+ treatment increased expression of GIRK4 from 0.48 ± 0.14- to 1.17 ± 0.10-fold ($n = 5$, $P = 0.007$) and nSREBP1 expression from 0.48 ± 0.09- to 1.75 ± 0.44-fold ($n = 5$, $P = 0.007$; Fig. 7*D* and *E*). Thus Li^+-treatment reversed the effects of insulin deficiency on I_{KACh} and gene expression.

Effect of the GSK3 Inhibitor CHIR-99021 on Autonomic Dysfunction and GIRK4 Expression

Although Li^+ has been shown to inhibit GSK3β function, it also inhibits (34) inositol monophosphatase and structurally related phosphomonoesterases as well as β-arrestin-2–Akt complex formation (34). Furthermore, studies have shown that Li^+ competes for Na^+ and affects membrane potential and Na^+ currents (35) as well as ventricular repolarization (36,37). For these reasons, we studied the effect of a specific GSK3β inhibitor, CHIR-99021, an aminopyrimidine that competitively inhibits GSK3 activity by competition with binding of ATP to the ATP-binding site (37). The time course of increase in the HF fraction in response to the injection of propranolol was computed before and after a 14-day treatment with 50 mg/kg CHIR-99021 given intraperitoneally daily (Fig. 8*A*). At 15 min after the propranolol injection, the 2-min average HF fraction increased from $46.8 \pm 2.9\%$ before CHIR-99021 treatment to $67.8 \pm 5.1\%$ after CHIR-99021 treatment ($n = 6$, $P = 0.034$; Fig. 8*B*). There was no significant difference in the decrease in mean heart rate in response to propranolol in Akita mice before and after CHIR-99021 treatment, consistent with the conclusion that CHIR-99021 had no effect on the sympathetic response of the heart (see Supplementary Table 4). The baseline HF fraction was not significantly different before and after CHIR-99021 treatment (data not shown). Western blot analysis of atrial homogenates demonstrated that GIRK4 expression was decreased in the atria of placebo-treated Akita mice to 0.28 ± 0.06-fold ($n = 6$, $P = 0.00002$) of levels in WT mice, whereas CHIR-99021 treatment increased GIRK4 levels from 0.28 ± 0.06- to 1.08 ± 0.14-fold ($n = 5$) of those in WT mice, which was significantly higher than in placebo ($P = 0.0003$). Finally, compared with WT, SREBP-1 in placebo-treated Akita mice was decreased to 0.53 ± 0.07-fold ($n = 6$, $P = 0.006$), whereas treatment of Akita mice with CHIR-99021 increased SREBP-1 from 0.53 ± 0.07- to 1.17 ± 0.11-fold ($n = 5$, $P = 0.0008$; Fig. 8*C* and *D*). These data strongly support the role of hyperactivity of GSK3β in autonomic dysfunction in the type 1 diabetic Akita mouse.

DISCUSSION

Cardiac parasympathetic dysfunction has been described in a number of animal models for diabetes. Baroreceptor-mediated bradycardia was impaired in diabetic rabbits (38). HRV was decreased in streptozotocin-treated rats (39) in association with degeneration of autonomic neurons (40) and decreased autonomic responsiveness of the heart. Thus, studies have implicated neuronal dysfunction and/or abnormalities of the response of the heart to parasympathetic signaling in the pathogenesis of parasympathetic dysfunction (41).

We previously presented data demonstrating that parasympathetic dysfunction in the type 1 diabetic heart is at least partly due to decreased expression of proteins in atrial myocytes that mediate the response of the heart to parasympathetic stimulation (20). Here we demonstrate a molecular mechanism for a novel relationship between the insulin-signaling pathway and the regulation of the response of the heart to parasympathetic stimulation in the atrial myocardium. These data demonstrate that insulin regulates the expression of the GIRK4 subunit of I_{KACh}, which is responsible for the hyperpolarization and resulting negative chronotropic response of the heart to parasympathetic stimulation by an SREBP-1–dependent mechanism. Although studies of the function of GSK3β are limited by the lack of inhibitors that differentiate between GSK3α and GSK3β, a combination of experiments using the GSK3 inhibitor Kenpaullone, which increases SREBP-1 and GIRK4, and the overexpression of a DA-GSK3β, which interferes with the expression of SREBP-1 and GIRK4, strongly supports the conclusion that GSK3β plays a role in the regulation of their expression. Taken together with the finding that decreased insulin levels in the Akita mouse result in a marked decrease in p-GSK3β and a resulting hyperactivity of GSK3β, these data support the conclusion that the decreased expression of SREBP-1 and GIRK4 in the Akita mouse is at least partly due to increased GSK3β activity. The physiologic relevance of GSK3β regulation of SREBP-1 and GIRK4 is supported by the finding that Kenpaullone treatment of HL-1 cells increases not only the levels of SREBP-1 and GIRK4 but also the activity of I_{KACh}.

Furthermore, the decrease in HF fraction and the attenuated negative chronotropic response to parasympathetic stimulation in the Akita type 1 diabetic mouse and the decrease in I_{KACh} in atrial myocytes from the

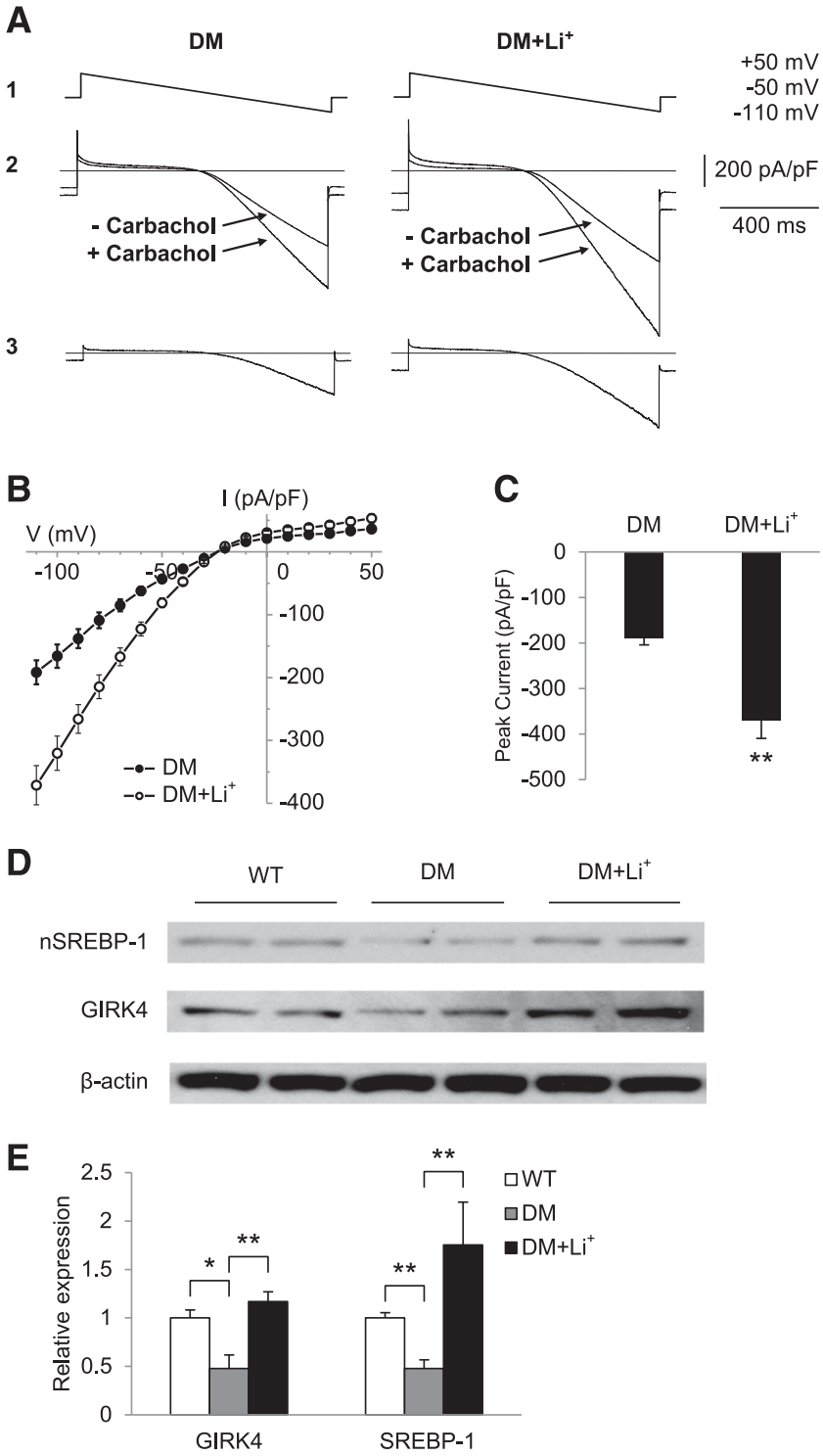

Figure 7—Li^+ treatment increases I_{KACh} in atrial myocytes and increases levels of nSREBP-1 and GIRK4 expression in the Akita atrium. I_{KACh} was determined as described in RESEARCH DESIGN AND METHODS, and I-V plots were constructed. *A*: I-V relationship of the carbamylcholine-induced whole-cell currents elicited from a 1-s voltage ramp with a continuously changing voltage from +50 to −110 mV (1); current from a typical atrial myocyte with and without 20 μmol/L carbamylcholine (2), and current generated by subtracting the trace obtained before and after the addition of carbamylcholine (3). *B*: I-V plots constructed from a series of data points as in *A*3. Data are the mean ± SEM of 12 recordings each from cells from four untreated Akita mice and four Li^+-treated Akita mice. *C*: Quantitation of peak inward currents from *A*. $^{**}P = 0.006$ compared with control. *D*: Levels of nSREBP-1 and GIRK4 in atria from WT, DM and Li^+-treated Akita diabetic mice (DM+Li^+) determined by Western blot analysis of atrial extracts of 2 mice in each group. *E*: Densitometric analysis of nSREBP-1 and GIRK4; 5 mice in each group determined as in *D*. Data were normalized to the expression of β-actin. $^{*}P < 0.05$, $^{**}P < 0.01$.

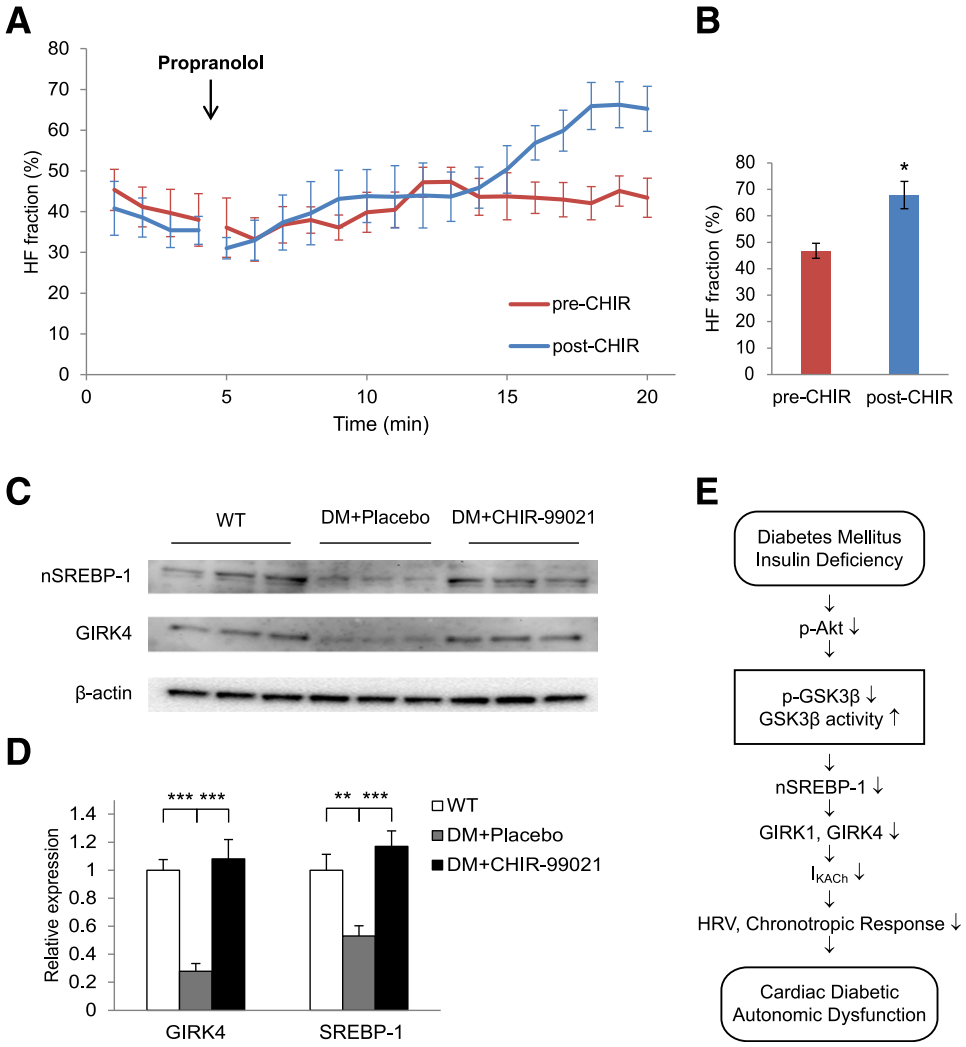

Figure 8—The GSK3β inhibitor CHIR-99021 increases HF fraction and levels of expression of nSREBP-1 and GIRK4 in Akita mice. *A*: Composite plots of the averaged (± SEM) time course of the increase in HF fraction after injection of propranolol in mice before and after treatment with CHIR-99021. *B*: Comparison of the magnitude of HF fraction pre–CHIR-99021 and post–CHIR-99021 computed 15 min after propranolol injection. CHIR-99021 had no effect on baseline HF fraction (data not shown). For these experiments, each mouse served as its own control. *C:* Levels of nSREBP-1 and GIRK4 in atria from WT, placebo (DM + Placebo), and CHIR-99021–treated Akita mice (DM + CHIR-99021) determined by Western blot analysis. *D:* Densitometric analysis of nSREBP-1 and GIRK4 from *C*. Data were normalized to the expression of β-actin. *E:* Schematic representation of the proposed effect of hypoinsulinemia on GSK3β and the development of parasympathetic dysfunction. $^{*}P < 0.05$, $^{**}P < 0.01$, $^{***}P < 001$.

Akita mouse were partly reversed by treatment of mice with Li^+, an inhibitor of GSK3β, in parallel with an increase in levels of atrial nSREBP-1 and GIRK4. Although the interpretation of the Li^+ data are complicated by effects on membrane potential and Na^+ currents (34–36), the role of GSK3β in the regulation of HRV and expression of genes involved in the parasympathetic response of the heart were corroborated by studies in Akita mice treated with CHIR-99021, a more specific GSK3β inhibitor that also increased the HF fraction and the expression of nSREBP-1 and GIRK4.

The finding that neither Li^+ nor CHIR-99021 had an effect on glucose levels (see Supplementary Table 1), taken together with our prior observation that increased SREBP-1 levels in insulin-treated Akita mice was not mimicked by phloridzin treatment, which normalizes glucose levels by inhibiting glucose reuptake in the kidney, supported the conclusion that the decreased expression of genes involved in parasympathetic signaling reported here depends on hypoinsulinemia and not on hyperglycemia (20). These data strongly support the conclusion that parasympathetic dysfunction in the Akita mouse heart may be at least partly due to hyperactivity of GSK3β in response to decreased insulin levels, resulting in decreased nSREBP-1–dependent GIRK4 expression, attenuation of I_{KACh}, and a decrease in the HF fraction (Fig. 8*E*).

Modulation of heart rate response to parasympathetic simulation involves not only I_{KACh} but also the hyperpolarization-dependent $I_{(funny\ [f])}$ current as well as L-type Ca^{2+} currents. That L-type Ca^{2+} channel activity might be

decreased in the Akita mouse heart has been suggested (42). Such a decrease in L-type Ca^{2+} currents might affect the balance between the response of the heart rate to sympathetic and parasympathetic stimulation. However, unpublished data from our laboratory suggest that resting L-type Ca^{2+} currents are relatively unchanged in ventricular myocytes from Akita mice compared with WT mice. Although no data have appeared regarding $I_{(f)}$/HCN pacemaker currents in the Akita mouse heart, such a decrease in a hyperpolarization- dependent pacemaker current might also result in a decreased heart rate response to sympathetic stimulation. However, decreases in $I_{(f)}$ and/or L-type Ca^{2+} currents might decrease the response of the heart rate to sympathetic stimulation, thus attenuating the effect of parasympathetic dysfunction observed in these studies. Furthermore, our data demonstrate that the response of the heart to sympathetic stimulation is not decreased in the Akita mouse at the ages studied.

The impaired response of the heart to autonomic stimulation in patients with diabetes has been attributed to the development of neuronal dysfunction. These conclusions are based on the observations that autonomic dysfunction in animal and cell culture models of diabetes have demonstrated an increase in apoptosis in superior cervical ganglia, dorsal root ganglia, and Schwann cells from streptozotocin-treated rats. In vitro studies demonstrated increased caspase activity and an increase in reactive oxygen species under conditions of hyperglycemia that were reversed by IGF-I (43,44). More recently, Yang et al. (45) suggested that Akita mice might demonstrate abnormalities of autonomic innervation. Although direct measurements of vagal nerve function in the Akita mouse are beyond the scope of the studies reported here, our data do demonstrate a direct effect of insulin on the regulation of the expression of genes involved in the response of the heart to parasympathetic stimulation. Hence, although the decrease in HF fraction might be partly due to neuronal dysfunction, our data support the conclusion that the end organ might also demonstrate an impaired response to vagal stimulation because the increase in the HF fraction in Li^{+}-treated Akita mice was associated with increased expression of GIRK4 in the Akita atrium and an increase in I_{KACh} in atrial myocytes from the Akita mouse. The finding that patients with type 1 diabetes develop autonomic dysfunction in the presence of insulin replacement therapy might reflect the presence of irreversible neuropathy. Hence in our mouse model, early initiation of insulin treatment might attenuate the development of irreversible changes in innervation.

Given the role of insulin in the inhibition of GSK3β activity and the recent findings suggesting that GSK3β inhibitors might mimic the effects of insulin on glycogen synthase activity and gluconeogenesis in the liver (22), a role for hyperactivity of GSK3β in the pathogenesis of insulin resistance and the secondary effects of diabetes has been suggested. Thus, GSK3β has been implicated in the phosphorylation and proteosomal degradation of the insulin receptor substrate 1 in response to hyperglycemia and hence, might play a role in the development of insulin insensitivity (46). Recently, inhibition of GSK3β has been implicated in the replication and survival of pancreatic β-cells (47). Furthermore, hyperactive GSK3β has been implicated in the development of diabetic nephropathy and/or retinopathy (23). Our data are consistent with such a role of GSK3β in DAN. The relationship between GSK3β activity and the level of SREBP-1 in the hypoinsulinemic Akita mouse is consistent with recent findings demonstrating that GSK3β participates in regulating the phosphorylation, ubiquitination, and subsequent proteosomal degradation of SREBP-1 (48).

The analysis of heart rate and HRV has been complicated by the variation of activity levels in conscious mice. To minimize the effects of activity of the mice on HRV, we chose segments of the record for HRV analysis in which heart rate and frequency domain parameters were relatively stationary and noise caused by muscle activity and changes in entropy was minimal. We further developed a unique approach for the study of parasympathetic modulation of the heart rate by computing the HF fraction after the inhibition of the sympathetic contribution to the power spectrum in response to a propranolol injection. By using this approach, differences in the HF fraction after sympathetic blockade in WT and Akita mice would be due primarily to differences in the parasympathetic contribution to HF power. However, differential effects of propranolol between groups on sympathetic–vagal interactions at the neuroeffector junction in the sinoatrial node might complicate the interpretation of the HRV analysis.

Abnormalities of heart rate response to parasympathetic stimulation and decreased HRV have both been associated with cardiovascular disease. Specifically, parasympathetic stimulation of the heart has been shown to play a protective role in the development of arrhythmias and sudden death (49). Furthermore, the decreased HRV associated with DAN has been shown to be a significant risk factor for sudden death and cardiovascular disease (6,50–53). Taken together, these measurements of parasympathetic function are a critical predictor of clinical risk for sudden death and heart disease in the diabetic population. The finding that inhibition of GSK3β partly reverses the abnormality of HRV in the Akita mouse offers important new insight into the pathogenesis of DAN and the treatment and prevention of sudden death in the diabetic population.

Acknowledgments. The authors are grateful to Florence Wagner and Edward Holson, Stanley Center for Psychiatric Research, Broad Institute, Cambridge, MA, for synthesizing and providing CHIR-99021.

Funding. This work was supported by the JDRF advanced postdoctoral fellowship JDRF 10-2010-78 to Y.Z., and by National Institutes of Health grants R21-DK-079622 to H.-J.P. and HL-074876 to J.B.G. The cellular electrophysiology studies were done in the Tufts University School of Medicine Center for

Neuroscience Research, supported by National Institutes of Health grant P30-NS047243.

Duality of Interest. No potential conflicts of interest relevant to this article were reported.

Author Contributions. Y.Z. designed and performed most of the experiments and quantified the results in association with C.M.W., H.-J.P., and J.B.G. C.M.W. performed the statistical analyses, produced the figures, developed the concepts and design of the heart rate and HRV experiments, wrote the software, and analyzed the heart rate and HRV data. Y.Z., C.M.W., and J.B.G. wrote the manuscript. C.M.W. and K.L.P. performed Western blot analyses. K.L.P. generated the chick atrial myocyte cultures and performed the studies in HL-1 cells. C.D. carried out measurements of I_{KACh}, B.W. generated the atrial myocyte cultures, J.Q.P. supervised the synthesis and characterization of CHIR-99021 in the mouse and its application to these studies, and J.M.K. provided the Myr-Akt construct and was involved in the evaluation of signaling pathways. M.J.A. implanted ECG transmitters and assisted with measurements of heart rate. W.C.C. provided the HL-1 cells and advice on maintaining them in culture. R.M.B. performed the echocardiographic measurements and calculated left ventricular parameters. J.B.G. is the guarantor of this work and, as such, had full access to all the data in the study and takes responsibility for the integrity of the data and the accuracy of the data analysis.

Prior Presentation. Parts of this study were presented at the annual meeting of the American Autonomic Society, Marco Island, FL, 3–6 November 2010 and in Buzios, Brazil, 12–16 September 2011.

References

1. Aronson D, Rayfield EJ, Chesebro JH. Mechanisms determining course and outcome of diabetic patients who have had acute myocardial infarction. Ann Intern Med 1997;126:296–306

2. Brown DW, Giles WH, Greenlund KJ, Valdez R, Croft JB. Impaired fasting glucose, diabetes mellitus, and cardiovascular disease risk factors are associated with prolonged QTc duration. Results from the Third National Health and Nutrition Examination Survey. J Cardiovasc Risk 2001;8:227–233

3. Allessie MA, Lammers WJ, Bonke IM, Hollen J. Intra-atrial reentry as a mechanism for atrial flutter induced by acetylcholine and rapid pacing in the dog. Circulation 1984;70:123–135

4. Aronson D. Pharmacologic modulation of autonomic tone: implications for the diabetic patient. Diabetologia 1997;40:476–481

5. Valensi P, Paries J, Attali JR; French Group for Research and Study of Diabetic Neuropathy. Cardiac autonomic neuropathy in diabetic patients: influence of diabetes duration, obesity, and microangiopathic complications–the French multicenter study. Metabolism 2003;52:815–820

6. Heller S. Dead in bed. Diabet Med 1999;16:782–785

7. Logothetis DE, Kurachi Y, Galper J, Neer EJ, Clapham DE. The beta gamma subunits of GTP-binding proteins activate the muscarinic K+ channel in heart. Nature 1987;325:321–326

8. Vivaudou M, Chan KW, Sui JL, Jan LY, Reuveny E, Logothetis DE. Probing the G-protein regulation of GIRK1 and GIRK4, the two subunits of the KACh channel, using functional homomeric mutants. J Biol Chem 1997;272:31553–31560

9. Krapivinsky G, Gordon EA, Wickman K, Velimirović B, Krapivinsky L, Clapham DE. The G-protein-gated atrial K^+ channel IKACh is a heteromultimer of two inwardly rectifying K(+)-channel proteins. Nature 1995;374:135–141

10. Thomas SL, Chmelar RS, Lu C, Halvorsen SW, Nathanson NM. Tissue-specific regulation of G-protein-coupled inwardly rectifying K^+ channel expression by muscarinic receptor activation in ovo. J Biol Chem 1997;272:29958–29962

11. Pertovaara A, Ostergård M, Ankö ML, et al. RFamide-related peptides signal through the neuropeptide FF receptor and regulate pain-related responses in the rat. Neuroscience 2005;134:1023–1032

12. Dobrev D, Graf E, Wettwer E, et al. Molecular basis of downregulation of G-protein-coupled inward rectifying K(+) current (I(K,ACh) in chronic human atrial fibrillation: decrease in GIRK4 mRNA correlates with reduced I(K,ACh) and muscarinic receptor-mediated shortening of action potentials. Circulation 2001;104:2551–2557

13. Brown MS, Ye J, Rawson RB, Goldstein JL. Regulated intramembrane proteolysis: a control mechanism conserved from bacteria to humans. Cell 2000;100:391–398

14. Matsuda M, Korn BS, Hammer RE, et al. SREBP cleavage-activating protein (SCAP) is required for increased lipid synthesis in liver induced by cholesterol deprivation and insulin elevation. Genes Dev 2001;15:1206–1216

15. Foretz M, Guichard C, Ferré P, Foufelle F. Sterol regulatory element binding protein-1c is a major mediator of insulin action on the hepatic expression of glucokinase and lipogenesis-related genes. Proc Natl Acad Sci USA 1999;96:12737–12742

16. Park HJ, Kong D, Iruela-Arispe L, Begley U, Tang D, Galper JB. 3-hydroxy-3-methylglutaryl coenzyme A reductase inhibitors interfere with angiogenesis by inhibiting the geranylgeranylation of RhoA. Circ Res 2002;91:143–150

17. Park HJ, Georgescu SP, Du C, et al. Parasympathetic response in chick myocytes and mouse heart is controlled by SREBP. J Clin Invest 2008;118:259–271

18. Kayo T, Koizumi A. Mapping of murine diabetogenic gene mody on chromosome 7 at D7Mit258 and its involvement in pancreatic islet and beta cell development during the perinatal period. J Clin Invest 1998;101:2112–2118

19. Mathews CE, Langley SH, Leiter EH. New mouse model to study islet transplantation in insulin-dependent diabetes mellitus. Transplantation 2002;73:1333–1336

20. Park HJ, Zhang Y, Du C, et al. Role of SREBP-1 in the development of parasympathetic dysfunction in the hearts of type 1 diabetic Akita mice. Circ Res 2009;105:287–294

21. Rylatt DB, Aitken A, Bilham T, Condon GD, Embi N, Cohen P. Glycogen synthase from rabbit skeletal muscle. Amino acid sequence at the sites phosphorylated by glycogen synthase kinase-3, and extension of the N-terminal sequence containing the site phosphorylated by phosphorylase kinase. Eur J Biochem 1980;107:529–537

22. Lee J, Kim MS. The role of GSK3 in glucose homeostasis and the development of insulin resistance. Diabetes Res Clin Pract 2007;77(Suppl. 1):S49–S57

23. Wagman AS, Nuss JM. Current therapies and emerging targets for the treatment of diabetes. Curr Pharm Des 2001;7:417–450

24. De Sarno P, Axtell RC, Raman C, Roth KA, Alessi DR, Jope RS. Lithium prevents and ameliorates experimental autoimmune encephalomyelitis. J Immunol 2008;181:338–345

25. Gehrmann J, Hammer PE, Maguire CT, Wakimoto H, Triedman JK, Berul CI. Phenotypic screening for heart rate variability in the mouse. Am J Physiol Heart Circ Physiol 2000;279:H733–H740

26. Thireau J, Zhang BL, Poisson D, Babuty D. Heart rate variability in mice: a theoretical and practical guide. Exp Physiol 2008;93:83–94

27. Task Force of the European Society of Cardiology and the North American Society of Pacing and Electrophysiology. Heart rate variability: standards of measurement, physiological interpretation and clinical use. Circulation 1996;93:1043–1065

28. DeHaan RL. Development of form in the embryonic heart. An experimental approach. Circulation 1967;35:821–833

29. Barnett JV, Haigh LS, Marsh JD, Galper JB. Effects of low density lipoproteins and mevinolin on sympathetic responsiveness in cultured chick atrial cells. Regulation of beta-adrenergic receptors and αs. J Biol Chem 1989;264:10779–10786

30. Park HJ, Begley U, Kong D, et al. Role of sterol regulatory element binding proteins in the regulation of Galpha(i2) expression in cultured atrial cells. Circ Res 2002;91:32–37

31. Bain J, McLauchlan H, Elliott M, Cohen P. The specificities of protein kinase inhibitors: an update. Biochem J 2003;371:199–204

32. Doble BW, Woodgett JR. Role of glycogen synthase kinase-3 in cell fate and epithelial-mesenchymal transitions. Cells Tissues Organs 2007;185:73–84

33. Claycomb WC, Lanson NA Jr, Stallworth BS, et al. HL-1 cells: a cardiac muscle cell line that contracts and retains phenotypic characteristics of the adult cardiomyocyte. Proc Natl Acad Sci USA 1998;95:2979–2984
34. O'Brien WT, Klein PS. Validating GSK3 as an in vivo target of lithium action. Biochem Soc Trans 2009;37:1133–1138
35. Darbar D, Yang T, Churchwell K, Wilde AA, Roden DM. Unmasking of brugada syndrome by lithium. Circulation 2005;112:1527–1531
36. Hunter DR, Haworth RA, Berkoff HA. Cellular lithium uptake as a probe of sodium channels in the rat heart: modulation of lithium uptake by tetrodotoxin, verapamil, anthopleurin-A, isoproterenol and external stimulation. J Mol Cell Cardiol 1984;16:1083–1090
37. Bain J, Plater L, Elliott M, et al. The selectivity of protein kinase inhibitors: a further update. Biochem J 2007;408:297–315
38. McDowell TS, Hajduczok G, Abboud FM, Chapleau MW. Baroreflex dysfunction in diabetes mellitus. II. Site of baroreflex impairment in diabetic rabbits. Am J Physiol 1994;266:H244–H249
39. Fazan R Jr, Ballejo G, Salgado MC, Moraes MF, Salgado HC. Heart rate variability and baroreceptor function in chronic diabetic rats. Hypertension 1997; 30:632–635
40. De Angelis K, Schaan BD, Maeda CY, Dall'Ago P, Wichi RB, Irigoyen MC. Cardiovascular control in experimental diabetes. Braz J Med Biol Res 2002;35: 1091–1100
41. Van Buren T, Schiereck P, De Ruiter GJ, Gispen WH, De Wildt DJ. Vagal efferent control of electrical properties of the heart in experimental diabetes. Acta Diabetol 1998;35:19–25
42. Lu Z, Jiang YP, Xu XH, Ballou LM, Cohen IS, Lin RZ. Decreased L-type Ca2+ current in cardiac myocytes of type 1 diabetic Akita mice due to reduced phosphatidylinositol 3-kinase signaling. Diabetes 2007;56:2780–2789
43. Russell JW, Feldman EL. Insulin-like growth factor-I prevents apoptosis in sympathetic neurons exposed to high glucose. Horm Metab Res 1999;31:90–96
44. Russell JW, Sullivan KA, Windebank AJ, Herrmann DN, Feldman EL. Neurons undergo apoptosis in animal and cell culture models of diabetes. Neurobiol Dis 1999;6:347–363
45. Yang B, Chon KH. Assessment of diabetic cardiac autonomic neuropathy in type I diabetic mice. Conf Proc IEEE Eng Med Biol Soc 2011:6560–6563
46. Liberman Z, Plotkin B, Tennenbaum T, Eldar-Finkelman H. Coordinated phosphorylation of insulin receptor substrate-1 by glycogen synthase kinase-3 and protein kinase C betall in the diabetic fat tissue. Am J Physiol Endocrinol Metab 2008;294:E1169–E1177
47. Mussmann R, Geese M, Harder F, et al. Inhibition of GSK3 promotes replication and survival of pancreatic beta cells. J Biol Chem 2007;282:12030–12037
48. Sundqvist A, Bengoechea-Alonso MT, Ye X, et al. Control of lipid metabolism by phosphorylation-dependent degradation of the SREBP family of transcription factors by SCF(Fbw7). Cell Metab 2005;1:379–391
49. Schwartz PJ, Billman GE, Stone HL. Autonomic mechanisms in ventricular fibrillation induced by myocardial ischemia during exercise in dogs with healed myocardial infarction. An experimental preparation for sudden cardiac death. Circulation 1984;69:790–800
50. Kataoka M, Ito C, Sasaki H, Yamane K, Kohno N. Low heart rate variability is a risk factor for sudden cardiac death in type 2 diabetes. Diabetes Res Clin Pract 2004;64:51–58
51. Jouven X, Empana JP, Schwartz PJ, Desnos M, Courbon D, Ducimetière P. Heart-rate profile during exercise as a predictor of sudden death. N Engl J Med 2005;352:1951–1958
52. Burger AJ, Charlamb M, Sherman HB. Circadian patterns of heart rate variability in normals, chronic stable angina and diabetes mellitus. Int J Cardiol 1999;71:41–48
53. Valensi PE, Johnson NB, Maison-Blanche P, Extramania F, Motte G, Coumel P. Influence of cardiac autonomic neuropathy on heart rate dependence of ventricular repolarization in diabetic patients. Diabetes Care 2002;25:918–923